Decadal-scale variations in ice flow along Whillans Ice Stream and its tributaries, West Antarctica

Leigh A. STEARNS,* Kenneth C. JEZEK, C.J. VAN DER VEEN

Byrd Polar Research Center and Department of Geological Sciences, The Ohio State University, 1090 Carmack Road, Columbus, Ohio 43210-1002, USA
E-mail: leigh.stearns@maine.edu

ABSTRACT. We investigate velocity changes occurring along Whillans Ice Stream (WIS) by comparing velocities derived from repeat aerial photographs acquired in 1985–89 (average date of 1987) to interferometric satellite radar (InSAR) velocities collected in 1997. Three different analysis methods are applied to the velocity data. First, temporal and spatial changes in velocities are correlated to identifiable features (flowlines, shear margins, bed features) visible on the 1997 RADARSAT Antarctic Mapping Project mosaic. Second, we relate velocity gradients to stresses via the flow law and, along with surface topography and ice-thickness data, apply the force-budget technique to determine the relative importance of driving stress, side drag and basal drag over time. Finally, the mass balance of the main part of WIS is determined for 1987 and 1997. Our results are consistent with previous studies that show an overall deceleration resulting in downstream thickening of the ice stream (Whillans and others, 2001; Joughin and others, 2002).

1. INTRODUCTION

There is a growing body of evidence suggesting that the Siple Coast ice streams, West Antarctica, are evolving on centennial and even decadal time-scales (Clarke and Bentley, 1995, 2000; Van der Veen and Whillans, 1996; Bindschadler and Vornberger, 1998; Harrison and others, 1998; Jacobson and Raymond, 1998; Echelmeyer and Harrison, 1999; Joughin and others, 2002). Understanding and predicting the future behavior of these ice streams is important because discharge from the West Antarctic ice sheet (WAIS) is dominated by ice-stream flow. Changes in the flow dynamics of ice streams therefore play a large role in the mass balance of the entire ice sheet and have the potential for affecting sea level (Oppenheimer, 1998; Joughin and Tulaczyk, 2002).

Recent studies show that Kamb Ice Stream (former Ice Stream C) stopped approximately 140 years BP; Whillans Ice Stream (WIS; former Ice Stream B) is widening and decelerating; Bindschadler (former Ice Stream D) and Echelmeyer (former Ice Stream F) ice streams are thickening; and MacAyeal Ice Stream (former Ice Stream E) is thinning (Stephenson and Bindschadler, 1988; Retzlaff and others, 1993; Bindschadler and Vornberger, 1998; Hamilton and others, 1998; Echelmeyer and Harrison, 1999; Joughin and Tulaczyk, 2002; Joughin and others, 2002). Deceleration estimates along WIS range from 2.1–2.6 m a^{-2} along the trunk to 5.0–19.0 m a^{-2} along the ice plain (Stephenson and Bindschadler, 1988; Hulbe and Whillans, 1997; Bindschadler and Vornberger, 1998; Echelmeyer and Harrison, 1999; Joughin and others, 2002). There is clear evidence that the mass balance of WIS is changing, but quantitative assessments of the rate of change vary by an order of magnitude (Shabtaie and others, 1988; Whillans and Bindschadler, 1988; Joughin and Tulaczyk, 2002). Whillans and Bindschadler (1988) calculated a thickness change of -0.06 ± 0.04 m a^{-1} using updated accumulation rates and Transit satellite velocity measurements across a specified gate. Using different Transit velocities and widely spaced accumulation rate measurements, Shabtaie and others (1988) calculated a dramatic thickness change of -0.06 ± 0.1 m a^{-1} for an area upstream of the merger of WIS with Van der Veen Ice Stream (VIS; former Ice Stream B1). Joughin and Tulaczyk (2002) estimated a net balance of 0.034 ± 0.037 m a^{-1} for the same area based on a dense array of interferometric (InSAR) velocities. In this paper, we compare these InSAR velocities to photogrammetric velocities collected 10 years earlier. Our goal is to determine whether surface velocities (and subsequently mass-balance estimates) change uniformly along the length of the ice stream, and uniformly across both major tributaries, or whether changes are concentrated in certain areas.

2. DATA

We use two remotely sensed velocity datasets in this study: one derived from repeat aerial photography from 1985–89 (Jackson, 1991; Whillans and others, 1993) and the other based on synthetic aperture radar interferometry (InSAR) from the 1997 RADARSAT Antarctic Mapping Project (RAMP: Jezek, 1999; Joughin and others, 2002). Ice-thickness data from BEDMAP (Lythe and others, 2000) and accumulation rates from Venteris and Whillans (1998) are used to solve the mass-balance equation. For the force-budget analysis, surface topography is from the Ohio State University digital elevation model (OSU DEM: Jezek and others, 1999; Liu and others, 1999) and bed topography is from BEDMAP (Lythe and others, 2000).

2.1. Photoblock data

Repeat aerial photography was used to obtain closely spaced velocity measurements along four sectors (herein referred to as 'photoblocks') of WIS and VIS (Whillans and others, 1993). Each photoblock consists of several aerial photographs linked together to produce a stereo model. The

*Present address: Climate Change Institute, University of Maine, 303 Bryand Global Sciences Center, Orono, Maine 04469, USA.

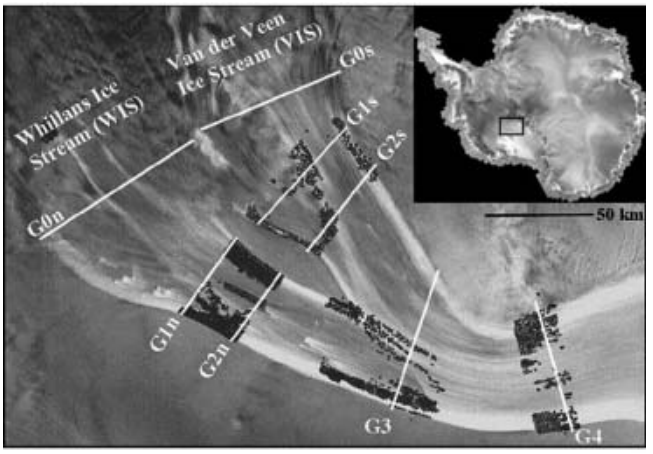

Fig. 1. The locations of photogrammetric velocity data points (black dots) overlain on a portion of the RAMP mosaic. The transects used in this study are shown in white.

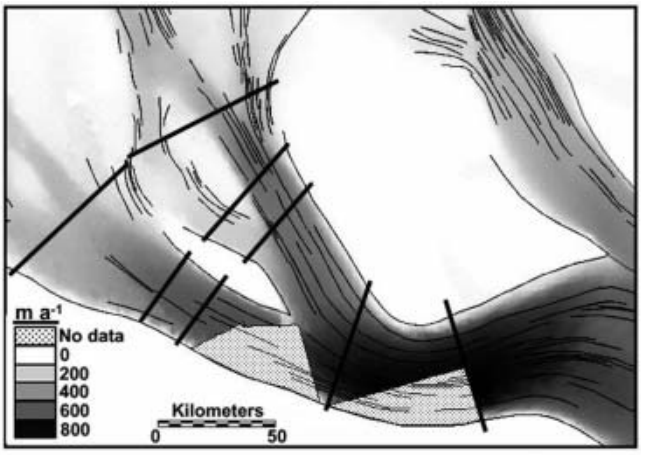

Fig. 2. InSAR velocities for WIS and VIS. Velocities <50 m a^{-1} are white, and areas with no data are speckled. Thick black lines spanning the ice stream represent transects used in this study (labeled in Fig. 1). Thin black lines trending down the ice stream are flowlines traced from the RAMP mosaic.

photo mosaic is constrained by Transit satellite ground-control stations and image overlap. The locations of velocities derived within each photoblock are shown in Figure 1, overlain on a RADARSAT image.

The aerial photographs are tied to ground-control stations on ridge ice and on the fast-moving ice stream. Network adjustment techniques were applied to improve the precision of fast-moving stations, the details of which are summarized in McDonald and Whillans (1988, 1992) and Whillans and others (1993).

To derive velocities from time-sequential photo-mosaics, the displacement of surface features (crevasses and drift mounds) observed in both mosaics was measured (Jackson, 1991; Whillans and others, 1993). As a result, the distribution of velocity data is irregular throughout the block and absent in the crevasse-free center of the ice stream. In order to obtain a more uniform distribution of velocities, a cubic spline with an r^2 of 0.954 was fit to a cluster of ten transects.

Errors associated with the photoblock velocities can originate from the photogrammetric measurements (1.7 m a^{-1}), ground-control points (0.4 m a^{-1}), or coordinate transformation (Whillans and others, 1993). Following Whillans and others' (1993) approximation, a total velocity uncertainty of 4.0 m a^{-1} is used in this study.

2.2. InSAR data

InSAR is a widely used technique for measuring ice-sheet surface velocities. As part of RAMP (Jezek, 1999), interferometric data were acquired for selected areas, including portions of the Siple Coast ice streams. Surface motion can be measured by analyzing the differences between coherently interfered pairs of complex synthetic aperture radar images, with the aid of a DEM. InSAR analysis, using a combination of interferometric and speckle matching methods (Joughin, 2002), provides closely spaced (500 m) velocity measurements across much of WIS and VIS (Fig. 2). The final dataset has a resolution range of 0.5–3.0 km, due to smoothing of the speckle-tracked data to reduce noise (Joughin, 2002).

There is a large degree of spatial variability in the InSAR errors across WIS. As Joughin (2002) points out, errors around the shear margins are inherently larger than in the interior of the ice stream (1σ errors are 1–4 m a^{-1}). For this study, the velocity and associated error (1–25 m a^{-1}) at each gridpoint along the specified transects was used in the mass-flux and force-budget calculations (see Joughin, 2002, for a more complete description of the InSAR errors).

Absolute control for InSAR data in this region was done using a select set of Transit satellite measurements collected by Whillans and others (1993). Because the photoblock velocities were tied to similar ground-control points, it is possible that the InSAR velocities and the photoblock velocities are no longer independent datasets. However, only control points in slow-flow zones on interstream ridges were used for the InSAR analysis (Joughin and others, 2002), so we assume minimal coupling between the photoblock and InSAR velocities compared in this paper.

2.3. Ancillary data

To complete mass-balance and force-budget calculations, we require estimates of accumulation rate, ice thickness and bed topography. Accumulation rates are derived from a gridded compilation of isolated point measurements, with errors of ~15% or 0.016 m a^{-1} ice equivalent (Venteris and Whillans, 1998). Based on these data, we assign a range of accumulation rates from 0.13 m a^{-1} at the upstream end (gates G0), to 0.11 m a^{-1} at the terminus (gates G3 and G4) (Fig. 1).

Shabtaie and others (1987) conducted airborne radar soundings of the ice sheet along a dense grid (nominal flight-line spacing in both horizontal directions was roughly 50 km) to measure surface topography and ice thickness (from which basal topography is inferred) over the Ross ice streams (Shabtaie and Bentley, 1988). These data were combined with isolated surveys and then gridded to form the BEDMAP compilation (Lythe and Vaughan, 2000). Errors of 25 m for bed topography and 18 m for ice thickness are used (Lythe and Vaughan, 2000). These datasets were only used to calculate the driving stress. To reduce errors, the driving stress was calculated at least ten times across each transect, the results were averaged and the standard deviation calculated.

The OSU DEM was used as an estimate of surface topography. It is an integration of different topographical

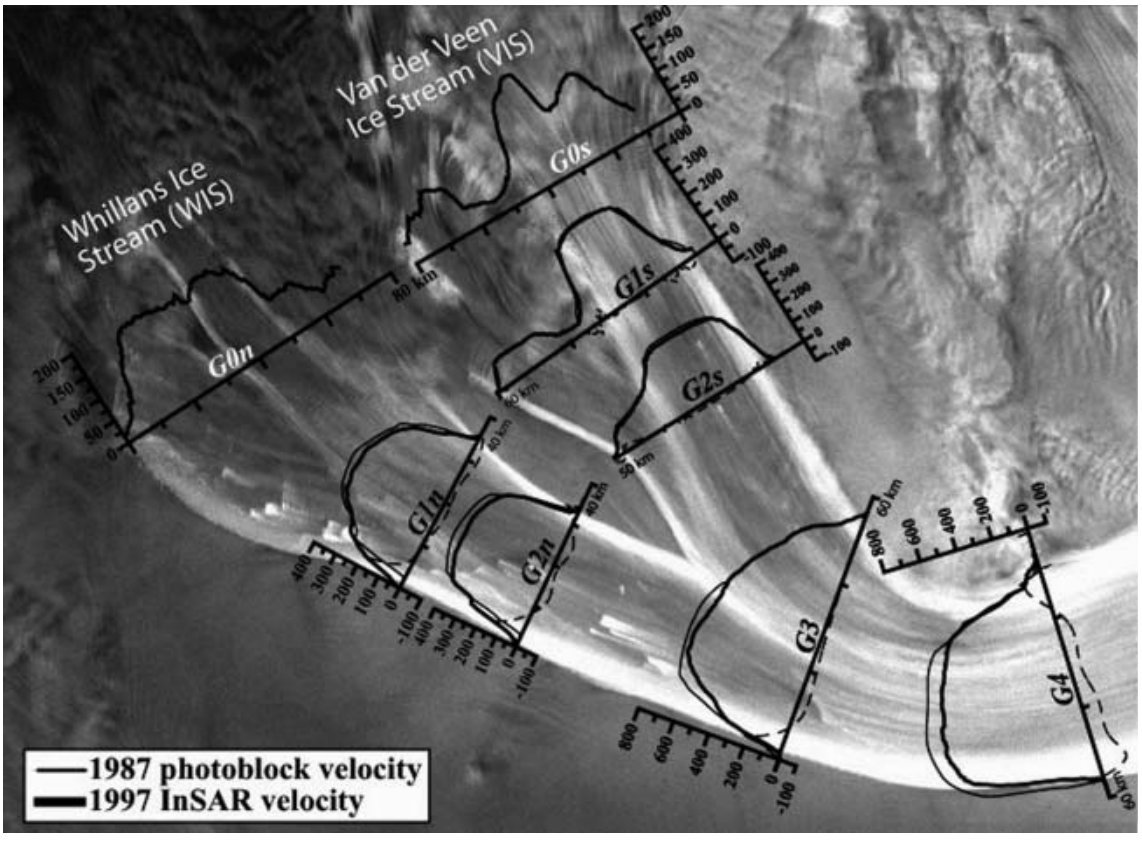

Fig. 3. Spatial and temporal changes in velocity ($m\,a^{-1}$) along WIS. The dotted line is the difference between the 1997 InSAR velocities and the 1987 photoblock velocities, plotted at the same scale. There are no photoblock data across transects G0n and G0s.

datasets of Antarctica combined into a single high-resolution DEM (Jezek and others, 1999; Liu and others, 1999). The vertical accuracy for the Ross ice streams is 15 m (Liu and others, 1999).

3. SPATIAL AND TEMPORAL CHANGES IN THE VELOCITY AND STRESS FIELDS

The flow of WIS has changed over the 10 year study interval, as we will illustrate by comparing the photoblock velocities (epoch 1987 on average) and InSAR velocities (epoch 1997). Margins have migrated, tributary widths have changed and velocities have decreased. These changes are a consequence of variations in the dominant stresses controlling the ice stream, which we determine from velocity gradients and the flow law.

3.1. Spatial and temporal variations in velocity

We compare velocities along transects perpendicular to flow (see Figs 1 and 2). The 1987 and 1997 velocities (both measured and interpolated) along these transects are shown in Figure 3. A shift in the limbs of the parabolic velocity profile is interpreted as a migration of the shear margin.

We begin with the upstream transects G0n and G0s. Ice velocities across the farthest upstream profiles (G0n and G0s) are characterized by the confluence of several smaller tributaries, which develop up-glacier of the main trunks (WIS and VIS). Both the velocity profiles and the RADARSAT mosaic show at least five tributaries dissected by the G0 transects. The southern tributaries are distinctly revealed in the velocity profiles as local velocity maxima and minima, while the northern tributaries are only weakly detected. These tributaries follow subglacial valleys, and therefore the processes that channel ice-stream flow are already well developed, especially across the northern transect (Studinger and others, 2001; Joughin and others, 2002). There are no velocities derived from the photoblocks in this region.

The 1987 and 1997 velocity profiles (transects G1n and G2n) across the main trunk of WIS are parabolic and symmetric about the center line. Over ten years, the trunk of WIS has decelerated an average of 2.9–4.1 $m\,a^{-2}$. This estimate is slightly higher than the average deceleration of 2.1–2.6 $m\,a^{-2}$ calculated in other studies (Hulbe and Whillans, 1997; Echelmeyer and Harrison, 1999; Joughin and others 2002).

Along VIS, the three original tributaries have reduced to two and are in the process of merging together, as can be seen by comparing transects G1s and G2s. There is a slight deceleration (0.6–1.7 $m\,a^{-2}$) with no associated shift in the margin. The velocity across transect G1s is faster than the downstream velocity at G2s. We speculate that this is due to the oblique intersection of a smaller channel (seen at the left edge of the G2s profile), resulting in an increase in longitudinal compressive stress.

At the distal end of the ice stream (profile G3), the branching network of ice-stream flow is reduced to one main trunk as WIS and VIS merge. The profile is roughly parabolic, with a velocity maximum of 688 $m\,a^{-1}$ biased towards the north end of the channel. We interpret this asymmetry as being due to the convergence of the two main tributaries and the effective narrowing of the northern branch by approximately 13 km (VIS has only narrowed 2 km at G3). At this location, ice deriving from the two tributaries (WIS and VIS) is separated by a clearly visible

suture zone coinciding with the asymmetry of the velocity profile. From 1987 to 1997, there was a deceleration along the northern portion of the ice stream of approximately 4.5 m a^{-2}. Possible reasons for the deceleration are addressed in section 6.2.

The velocity profile becomes more symmetric downstream at G4 where there is only slight evidence of the upstream tributaries in the velocity profile. That is, the velocity maximum remains displaced towards the northern margin, and velocities are somewhat smaller across the southern half of the transect. This likely reflects the generally lower speeds on VIS compared to WIS. More significantly, along this transect we observe a dramatic deceleration of 7.2 m a^{-2} over 10 years, with a 1.7 km shift inwards of the northern margin. This value compares well to a mean deceleration of 6.5 m a^{-2} calculated by Joughin and others (2002) over the same area.

3.2. Margin migration

The margins of an ice stream play an important role in the down-ice dynamics. Many modeling and field-based studies agree that the driving stress, τ_{dx}, along WIS is almost entirely supported by lateral drag (e.g. Echelmeyer and others, 1994; Jackson and Kamb, 1997; Whillans and Van der Veen, 1997; Harrison and others, 1998; Joughin and others, 2002). If this is true, then the velocity at the center of the ice-stream center line is proportional to the fourth power of the width of the ice stream, *W*, (Van der Veen, 1999) according to

$$U_{\text{centerline}} = \frac{2}{n+1}\left(\frac{\tau_{dx}}{BH}\right)^{n} W^{n+1}. \quad (1)$$

In this expression, *B* is a viscosity parameter that increases with depth; in the following calculations, a depth-weighted value (540 kPa a$^{1/3}$) is used. The flow-law exponent, *n*, is taken to equal 3.

Even a slight increase in ice-stream width could lead to a large increase in glacier speed. The deceleration along WIS occurs with both outward (G1n, G2n) and inward (G4) margin migrations, giving clues to different processes controlling the migrations.

To determine changes in the shear margin positions, the photoblock velocity profiles were compared to the RADARSAT mosaic. Since the InSAR data are smoothed by 1–3 km, a direct comparison of the two velocity profiles proved tenuous (Joughin, 2002). For the photoblock data, the shear margin was defined as the start of a sharp increase in velocity: a narrow and distinct zone (Raymond and others, 2001). For the RADARSAT mosaic, the shear margin was determined as the outer extent of the arcuate crevasses. Echelmeyer and Harrison (1999) noted that these crevasses coincided with the greatest jump in along-flow velocity.

Using this technique, we found significant margin migration along the northern flank of the ice stream. Transect G1n has migrated outwards (north) 2.8 km; transect G2n has migrated outwards 1.7 km; transect G4 has migrated inwards 1.6–2.2 km. Along the southern side of G1n and G2n, there is up to 250 m outward migration. There was no noticeable shift in the margins of VIS; however, this could be due to poor visibility of arcuate crevasses in the RADARSAT imagery.

The shear margins of WIS have been studied extensively using various theoretical and field measurements. Velocity profiles (Echelmeyer and Harrison, 1998), crevasse curvature methods (Vornberger and Whillans, 1990), temperature profiles (Harrison and others, 1998) and theoretical studies (Jacobson and Raymond, 1998) all suggest a 7–30 m a^{-1} outward migration of the southern margin of WIS, comparable to our findings. We find substantially higher migration rates for the northern margin of WIS: outwards 170–280 m a^{-1} at G1n and G2n; inwards 170 m a^{-1} at G4. The magnitudes of these estimates are comparable to those found by Bindschadler and Vornberger (1998). Rapid outward migration rates are mechanically possible if the bed under the ridge ice is still warm and wet from previous streaming flow (Bindschadler and Vornberger, 1998; Jacobson and Raymond, 1998). Fast inward margin migration (as seen at G4) is best explained by the advection of colder ice from adjacent ridges into the ice stream and is not unprecedented (Van der Veen and Whillans, 1996; Jacobson and Raymond, 1998; Raymond and others, 2001). Clarke and Bentley (2000) estimated an inward migration rate of 100 m a^{-1} for the south margin of WIS (near G1n/G2n) as it migrated from the 'Fishhook' starting ~200 years ago. Similarly, Jacobel and others (2000) suggested that the multiple scars on the north margin of Kamb Ice Stream indicate that the margin moved inward in rapid jumps.

The migration of a shear margin is dictated by the balance between inward flow of cold ice from adjacent ridges (which narrows the ice stream) and shear heating of the margins (which widens the ice stream as the ridge ice is warmed) (Van der Veen and Whillans, 1996; Bindschadler and Vornberger, 1998; Jacobson and Raymond, 1998; Raymond and others, 2001). Spatially stable ice-stream margins are unlikely, due to the delicate balance described above and the dynamic nature of ice streams. However, Jacobson and Raymond (1998) suggest that a stable width for an ice stream could be maintained if there is a geologically determined boundary that precludes further outward expansion. Basal troughs and minimal margin migration support findings that the margins of VIS are geologically bounded.

3.3. Spatial and temporal variations in lateral shear stress

Prior studies have revealed the dominance of side drag along the lateral margins in opposing the gravitational driving stress and, therefore, in controlling the flow dynamics of WIS (Bindschadler and others, 1987; Echelmeyer and others, 1994; Jackson and Kamb, 1997; Whillans and Van der Veen, 1997; Joughin and others, 2002). Using the two sets of velocity data, we investigate spatial and temporal changes in the role of lateral drag following the procedure outlined by Whillans and Van der Veen (1997) (cf. Van der Veen, 1999, section 5.5). That is, shear stresses, R_{xy}, are calculated solely from the shear strain rate (equal to one-half the transverse gradient in the downstream velocity, *U*) and Glen's flow law, so that:

$$R_{xy} = B\left(\frac{1}{2}\frac{\partial U}{\partial y}\right)^{\frac{1}{n}}. \quad (2)$$

The variables *B* and *n* are the same as used in Equation (1). Because vertical shear is negligible on fast-moving ice streams where most of the motion derives from basal sliding or deformation of a subglacial layer of weak sediment, the depth-averaged velocity as called for in Equation (2) may be taken as the measured surface velocity. Finally, in this calculation longitudinal stresses are assumed negligible based on previous research (Whillans and

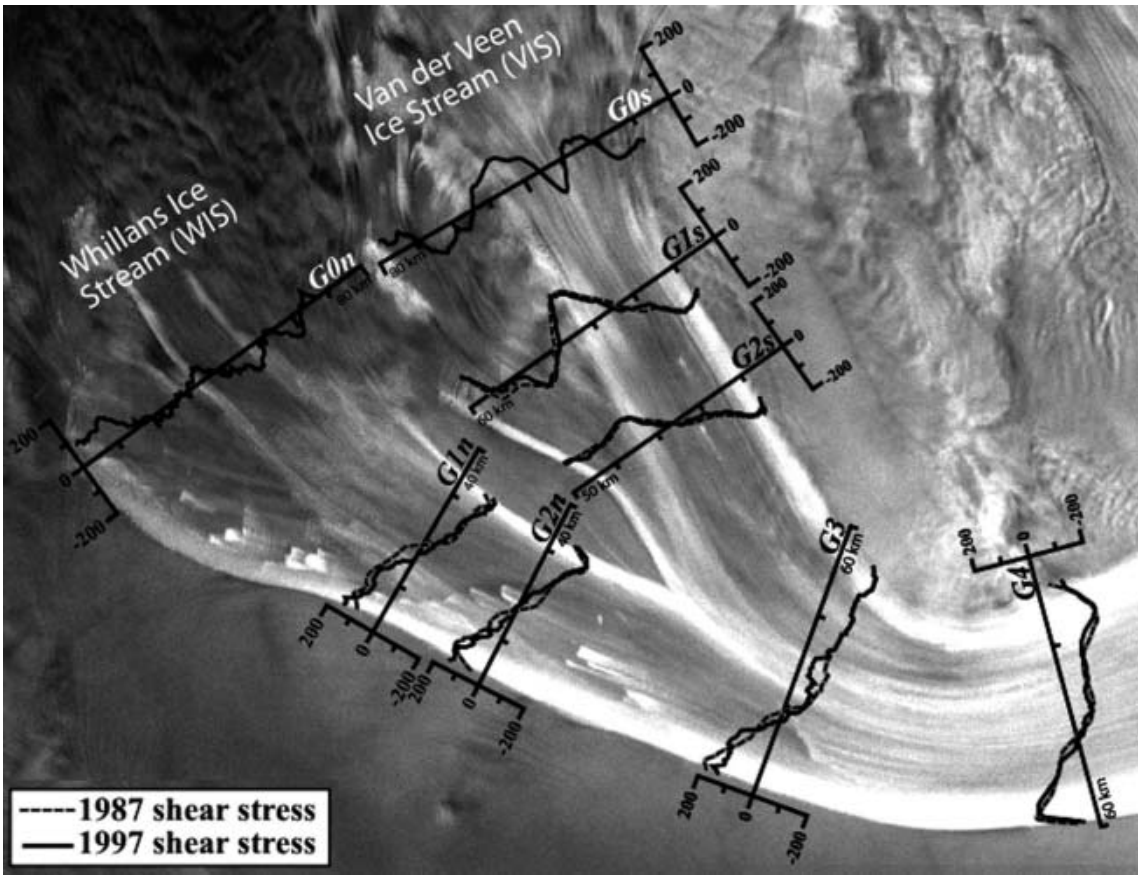

Fig. 4. Shear stress variations (kPa) across WIS, calculated from Equation (1). The 1987 shear stress is derived from the photoblock velocities, and the 1997 shear stress from InSAR velocities (as shown in Fig. 3).

Van der Veen, 1993) so that only the horizontal shear strain rate contributes to the effective strain rate. Calculated shear stress variations are shown in Figure 4.

Similar to the velocity field, the shear stress field simplifies as the effects of upstream tributaries attenuate and the ice stream approaches the Ross Ice Shelf. Across G0n/s, the shear stress fluctuates ~80 kPa above and below zero in response to merging tributaries of varying velocity. By G1n and G2n, the complex variations in shear stress observed at G0n/s have reduced to simple, near-linear variations in stress across the channel, characteristic of an area of the ice stream that is bounded by well-developed shear margins. A linear slope in shear stress is observed for both the InSAR and photoblock velocities. Because photoblock velocities are sparse away from the margins and because a cubic spline was fit to the photoblock velocity data points, the linearity of the shear stress slope could be artificial.

The situation at G2s and G3 is more complicated due to the confluence of nearby tributaries. For each of these profiles, the shear stress consists of a segment that is nearly constant with range and then abruptly changes to a segment that varies linearly. For both of these profiles the break point in slope is distinctly off-center. By G4, the pattern is again simplified to a near-linear variation in shear stress.

Temporal variations in shear stress are only noticeable in profiles G1n, G2n and G3 (Fig. 4). Along profiles G1n and G3 the variations appear to be spatially random. In G2n, there appears to be a systematic bias resulting from a decrease in shear stress along the northern portion of the profile.

4. STRESSES ON THE ICE STREAM

The large-scale mechanics controlling glacier flow can be determined by calculating the action effect of gravity and the subsequent resistance to it. Resistance can come from the bed, from the sides, or from along-flow obstacles. The goal of this section is to assess the dominant stresses acting on the ice stream over time.

Our calculation follows Van der Veen and Whillans (1989) who show that the depth-integrated force-balance equations resolve into terms involving averaged stresses and stress gradients. Here, a simple block-flow model is used, thereby assuming that stresses and strain rates are constant throughout the ice thickness (Van der Veen, 1999, section 5.5). The resulting equality between stresses and stress gradients is given by:

$$\tau_{dx} = \tau_{bx} - \left(\frac{\partial}{\partial x} HR_{xx}\right) - \left(\frac{\partial}{\partial y} HR_{xy}\right). \qquad (3)$$

The driving stress, τ_{dx}, is equated to gradients in resistive stresses which are the basal drag (τ_{bx}), differential longitudinal tension or compression (R_{xx}) and differential lateral drag (R_{xy}) (Whillans and others, 2000). H is the ice thickness. Whillans and Van der Veen (1993) conducted a thorough analysis of variations in longitudinal stresses along WIS and found these to be negligible (Echelmeyer and others, 1994; Jackson and Kamb, 1997; Whillans and Van der Veen, 1997; Harrison and others, 1998; Joughin and others, 2002). As a result, we consider longitudinal components to be negligible in our calculations. Basal drag is assumed to accommodate any residual imbalance between the driving stress and the differential lateral drag.

Table 1. Force budget along WIS in 1987 and 1997

Transect	Ice thickness m	Slope	Driving stress kPa	τ_w 1987 kPa	τ_w 1997 kPa	τ_{bx} 1987 kPa	τ_{bx} 1997 kPa
G0n–G1n	1060 ± 40	0.0014 ± 0.0008	13.3 ± 1.1	N/A	7.1 ± 0.9	N/A	6.2 ± 1.4
G0s–G1s	1502 ± 60	0.0029 ± 0.0005	39.2 ± 6.9	N/A	8.5 ± 1.3	N/A	30.7 ± 7.1
G1n–G3n	1042 ± 37	0.0014 ± 0.0001	13.1 ± 1.0	13.2 ± 2.9	11.8 ± 2.1	–0.1 ± 3.1	1.3 ± 2.3
G1s–G3s	1255 ± 72	0.0015 ± 0.0004	16.9 ± 4.6	11.1 ± 1.2	11.5 ± 1.8	5.8 ± 4.8	5.5 ± 4.9
G3–G4	932 ± 30	0.0014 ± 0.0001	11.7 ± 0.9	7.9 ± 1.7	7.2 ± 0.9	3.8 ± 1.9	4.5 ± 1.3

Lateral drag can be assessed by averaging the third term on the righthand side of Equation (3) from the margin to the center of the ice stream. The weighted lateral drag, τ_w on a section of the ice stream of width $2W$ is

$$\tau_w = \frac{H_w \tau_s}{W}, \quad (4)$$

where τ_s represents the lateral shear stress at the margins and H_w represents the thickness at the margins.

4.1. Spatial and temporal changes in the stresses

With the above assumptions, the force-balance equation is simplified to (Van der Veen, 1999, section 5.5):

$$\bar{\tau}_{dx} = \bar{\tau}_{bx} + \frac{H_w \tau_s}{W}. \quad (5)$$

Table 1 lists the values for each term in Equation (5) along sections of WIS and VIS bounded by transects calculated for 1987 and 1997. Before discussing the table, we note that there are two types of errors associated with the force-budget technique. First, there are errors that have propagated from the InSAR and photoblock velocities. Second, there are errors that are inherent in each dataset used: BEDMAP, the OSU DEM, and accumulation rates. The variance is computed by taking the partial derivative of each of the relevant equations discussed above. Errors are assumed to have a Gaussian distribution, and errors between variables are taken to be independent. We do not include an additional source of non-random error associated with assumptions in our model (e.g. neglecting the longitudinal stress gradients) and our averaging procedures.

The driving stress varies along the ice stream, as shown in Figure 5. To eliminate errors in deriving the driving stress, at least ten profiles (adjacent to each specified transect) were averaged for surface slope (RAMP DEM) and ice thickness (gridded BEDMAP) (Jezek and others, 1999; Liu and others, 1999; Lythe and Vaughan, 2000). For the surface slope, profiles greater than ten times the ice thickness were averaged and the standard deviation recorded (after Joughin and others, 2002). VIS has thicker ice and a steeper surface slope (see Table 1) and therefore supports a driving stress that is larger than the adjacent branch of WIS.

A change in the driving stress from 1987 to 1997 could explain some of the observed velocity and force-budget variations. As Joughin and others (2002) note, the surface velocity is very sensitive to changes in driving stress. Their calculated change in driving stress does explain their observed deceleration accounting for no, or minimal (up to 34 m a^{-1}), widening. Our estimates for widening are significantly larger: up to 300 m a^{-1}. In calculating the effect that thickening or thinning rates would have on the surface slope, we found that the prescribed elevation changes altered the driving stress by <1% of the total driving stress.

Figure 6 illustrates the respective distribution of basal shear stress and weighted lateral shear stress, as calculated from Equation (4). The weighted shear stress, τ_w, is relatively low (6.8–8.7 kPa) in the upper reaches of the ice stream, increases by 30–45% in the middle reach (to values of 9.8–14.7 kPa) and decreases back (6.9–10.4 kPa) near G4. There is a noticeable, but not statistically significant, temporal change in τ_w along the northern margin of WIS (near G2n and G4). In both of these locations, τ_w is reduced by ~2 kPa from 1987 to 1997. These are also the only two locations where there is a large shift in northern margin location, albeit in opposite directions. At G1n and G2n, the north margin migrates outward 1.7–2.8 km; at G4 the north margin migrates inward 1.6–2.2 km. This observation suggests that G4 is narrowing due to deceleration, while G1n and G2n are decelerating for another reason, possibly a change in basal conditions.

Values of calculated basal drag are not uniform throughout the ice stream. In the upstream portions of the ice stream, the driving stress is high (especially along VIS) but the calculated weighted shear stress is lower than the downstream values. This results in high values for calculated basal drag, based on Equation (5). This equation assumes that longitudinal components of stress are negligible, an invalid assumption at the tributaries (Price and others, 2002). Once the ice-stream shear margins become well developed in the middle section of the northern tributary, basal drag resists less of the driving stress, as anticipated (Echelmeyer and others, 1994; Jackson and Kamb, 1997; Whillans and Van der Veen, 1997; Harrison and others, 1998; Joughin and others, 2002). However, for VIS, basal drag is still an important component, accounting for 34% of the driving stress. The high basal drag estimate, however, could be a function of large errors in the RAMP DEM in this area (Joughin and others, 2002).

Along the main part of the WIS, basal drag is approximately 1–3 kPa, which agrees with estimates by Kamb (1991), Echelmeyer and others (1994) and Whillans and Van der Veen (1997). In these areas, basal drag opposes 15–30% of the driving stress, comparable to estimates by Joughin and others (2002). The remaining 70–85% of flow resistance is provided by lateral drag, highlighting the importance of the margins to ice-stream flow.

5. MASS BALANCE

Local rates of ice-sheet thickness change are computed using conservation of mass. We compute the net flux (F_{net}) by differencing the flux across the input gate (F_{in}) and the

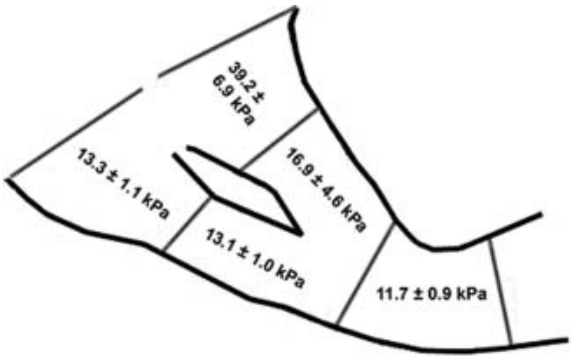

Fig. 5. The distribution of driving stress along WIS and VIS based on the OSU DEM and BEDMAP. The value above represents the mean driving stress for each area with a 2σ error, at an average date of 1999.

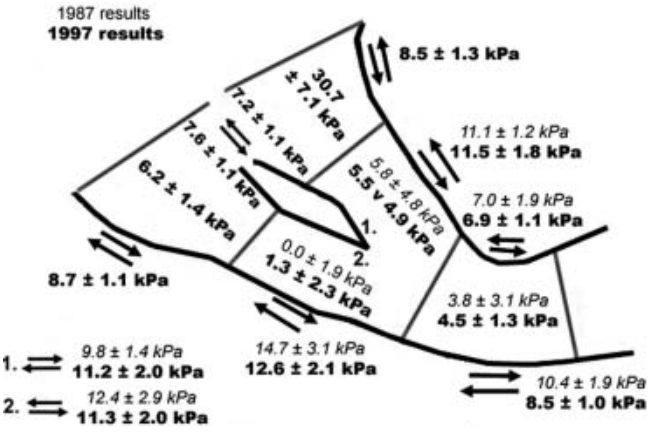

Fig. 6. Basal drag (italic labels in the center of the ice stream) and weighted shear stress values for 1987 (regular type) and 1997 (bold type).

flux across the output gate (F_{out}) of volume elements selected along the ice stream and using

$$F_{net} = F_{in} + F_r + F_l + F_{surf} - F_b - F_{out}. \quad (6)$$

Shear margins and flowlines were chosen as the lateral boundaries in the mass-balance calculation, in order to eliminate lateral flux contributions to the volume (F_r and F_l). While entrainment of ridge ice does occur across the shear margin, the flux is estimated to be <1% of the total flux and is therefore omitted in this study (Whillans and Van der Veen, 1993). The surface flux (F_{surf}) is calculated by integrating the estimated accumulation rate over the area defined by the flux gates and lateral margins. The basal flux, F_b, is assumed negative under WIS and VIS with estimates that range from a few millimeters (Budd and others, 1971) to several centimeters (Rose, 1979; Joughin and others, 2003) per year of melt. The basal flux is not necessarily negative, however, and freeze-on is reported to occur at the ice plain (~125 km down-glacier from G4) (Joughin and others, 2003). The basal flux is estimated through the basal melt-rate equation,

$$\frac{\Delta H}{\Delta t} = \frac{1}{\rho\lambda}\left(K\frac{\partial T}{\partial z} - \int \dot{\varepsilon}_{xz}\tau_{xz}\,dz - G - \tau_{bx}U\right), \quad (7)$$

which determines the rate of thickness change at the base. The melt rate depends on a number of variables (in order of their appearance in Equation (7)): latent heat of fusion, vertical heat conduction, strain heating, the geothermal heat flux, and potential heating. The values assigned to each parameter are listed in Table 2.

Evaluating Equation (7) with the values in Table 2 results in a basal melt rate that ranges from 1.4 to 28.8 mm a^{-1}. These values compare with model results of 0.5–6.8 mm a^{-1} by Joughin and others (2003). They are significantly less than the error limits assigned to each mass-balance flux, and this contribution to the mass budget is therefore neglected here.

The net flux difference is used to compute thickening rates in each of our sectors (Figs 7 and 8; data in the Appendix). The errors are computed using standard error analysis (Thomas and Bentley, 1978). We assign an error of 15% to the accumulation rate after Venteris and Whillans (1998). Velocity and ice-thickness errors are discussed above. Estimates for the error associated with choosing flow boundaries were negligible.

The overall state of balance is illustrated in Figures 7 and 8. In 1987 the estimated mass balance of WIS (the area between gates G1n/s and G4) was -0.42 ± 0.14 m a^{-1}. In 1997 the mass balance of a slightly larger area (including the G0 transects) was not significantly different from zero (-0.06 ± 0.16 m a^{-1}). Not only do our data suggest a regional change in mass balance over time, but they also indicate a spatial change as illustrated in Figures 7 and 8. For these figures, transects G3 and G4 were divided into G3n/s and G4n/s based on flowline boundaries.

In 1987 there was thinning along the entire length of the northern tributary. The largest thickness change was at the distal end at -0.70 ± 0.33 m a^{-1}. This is within the limits of Shabtaie and others' (1988) estimate of -1.30 ± 1.30 m a^{-1}

Table 2. Values of parameters used in Equation (7)

	Definition	Value	Source
ρ	Density of ice	917 kg m^{-3}	Van der Veen (1999, section 7.1)
λ	Latent-heat capacity of ice	3.34×10^5 J kg^{-1}	Van der Veen (1999, section 7.1)
K	Thermal conductivity of ice	2.1 W mK^{-1}	Van der Veen (1999, section 7.1)
$\partial T/\partial z>$	Heat conducted up from base	0.04 K m^{-1}	Engelhardt and others (1990)
ε_{xz}	Vertical strain rate	~0.00	This paper
τ_{xz}	Vertical shear stress	2.0 kPa	This paper
G	Geothermal heat flux	0.060 W m^{-2}	Whillans and others (1988)
τ_{bx}*	Basal shear stress	6.5, 46.1, 2.9, 7.4, 2.2 kPa	This paper
U*	Average velocity	200, 200, 400, 400, 800 m a^{-1}	This paper

*Values refer to transects G0n–G1n, G0s–G1s, G1n–G3n, G1s–G3s, G3–G4, respectively.

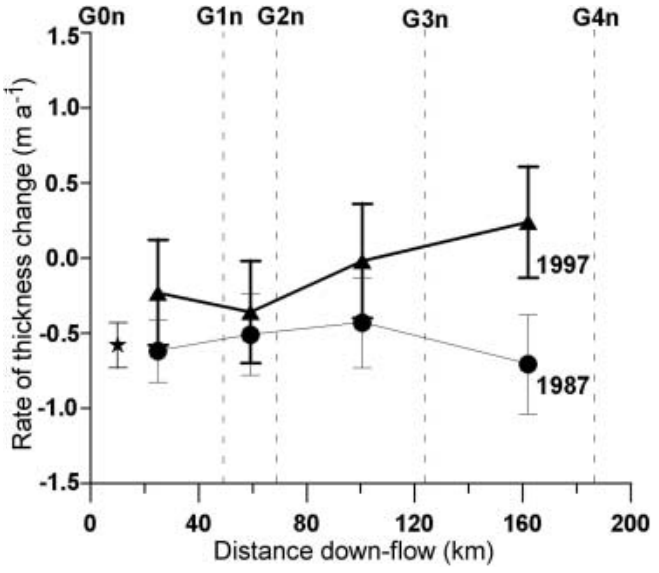

Fig. 7. Rate of thickness change, 1987–97, along WIS. The circles represent data from 1987, and the triangles data from 1997. Isolated stars are thinning rates estimated by Spikes and others (2003), using repeat laser altimetry (from 1997 and 1999) for an area slightly upstream of the study area.

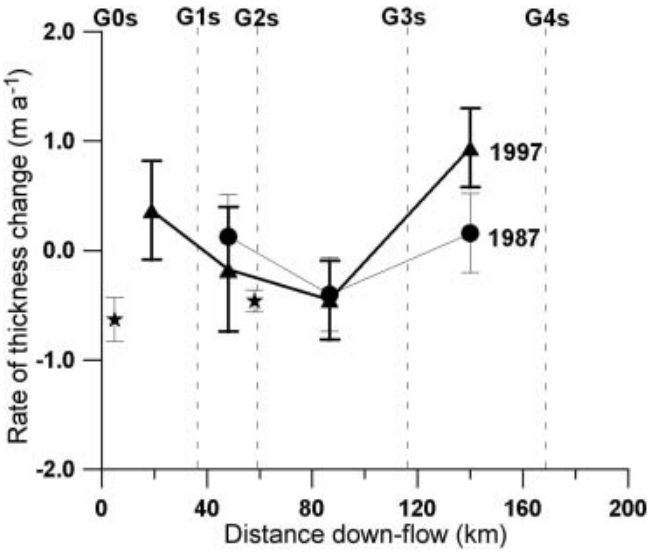

Fig. 8. Rate of thickness change, 1987–97, along VIS and the trunk of WIS. The circles represent data from 1987, and the triangles data from 1997. Isolated stars are thinning rates estimated by Spikes and others (2003), using repeat laser altimetry from 1997 and 1999.

for the same area (G3n–G4n). In 1997 the rate of thinning decreases with distance downstream and may in fact become positive at G4.

In contrast, VIS appears to be relatively close to balance, or thickening slightly at both the far upstream (G0s) and far downstream (G4s) ends. For the section near the confluence with the northern branch (between G2s and G3s), there is a minimum in the curve and the ice stream appears to be thinning. However, there is no statistical evidence for a temporal change in thickening except for the distal end (G4s) where thickening rates increase over time. This is true for both the northern and southern parts of the ice stream. Shabtaie and others' (1988) mass flux for VIS is considerably different. They found upstream thickness changes of $-1.26 \pm 0.37\,\mathrm{m\,a^{-1}}$ (between G0s and G1s) and downstream thickness changes of $1.20 \pm 1.30\,\mathrm{m\,a^{-1}}$ (between G3s and G4s). Because their data points were ground-based, their velocity profiles across each transect were determined by three to four points, and should be viewed with caution.

Many studies have charted the thickening and thinning rates of WIS, using a variety of datasets and techniques (Shabtaie and others, 1988; Whillans and Bindschadler, 1988; Joughin and Tulaczyk, 2002; Spikes and others, 2003). Using repeat laser altimetry, Spikes and others (2003) found the catchment areas of WIS to be thinning by roughly $1.0\,\mathrm{m\,a^{-1}}$ based on data collected in 1997–98 and 1999–2000. Joughin and Tulaczyk (2002), using the same InSAR velocities and accumulation rate data as in this study, integrated from the ice divide to the grounding line and found WIS to be thickening slightly. These results are by no means mutually exclusive since they are for different areas of the ice stream and, as our results show, each small segment of WIS and VIS has a distinct pattern of thinning/thickening.

6. DISCUSSION

WIS is evolving in space and time. In the 10 years considered in this study, the upstream segments and the southern tributary (VIS) have remained relatively stable while the northern tributary is widening and decelerating. Closer to the grounding line, however, the ice stream is narrowing and decelerating. While each section of the ice stream is changing uniquely, as a whole the changes tell a consistent story.

6.1. Summary of observations

Upstream gates (G0n, G0s)

Upstream, where ice-stream flow is not well developed, the velocity profiles are irregular. Many small tributaries are visible on the RADARSAT image, most without developed shear margins. These areas (especially near G0s) are characterized by high driving stresses and low lateral shear stresses. Here, longitudinal stress gradients may be important, potentially complicating some of our analyses (Price and others, 2002). Nonetheless, even with a component of longitudinal compression acting to resist the driving stress, basal drag values remain high (Joughin and others, 2002). Comparatively higher basal drag values combined with thicker ice imply more melt production beneath the tributaries than beneath the ice-stream trunk (Joughin and others, 2003). Thinning rates for 1997 (none exist for 1987) are not statistically different from zero.

WIS trunk (G1n, G2n)

Velocity and shear margin patterns indicate that the trunk of WIS is getting slower and wider over time. Common glaciological theory, expressed in Equation (1), states that ice-stream widening should produce a velocity increase. Because the opposite is true at both the WIS trunk and ice plain (125 km downstream from G4) (Bindschadler and Vornberger, 1998), Tulaczyk (2000) suggests that the velocity change was caused by a change in basal conditions rather than natural adjustments of the ice stream.

Our calculations show a ~2 kPa decrease in lateral drag along the northern margin where most of the changes occur. Basal drag, by default, increases. Despite the deceleration and widening in 1997, this section of the ice stream is still

discharging (slightly) more ice than it acquires, causing slight thinning. These observations support the hypothesis that deceleration at the WIS trunk is coincident with a change in basal conditions.

VIS trunk (G1s, G2s)

Few changes occur along VIS: the net flux is near zero, the margins are stable, the velocity is consistent and the stresses hardly change. This result is consistent with BEDMAP observations that the VIS may be bedrock-controlled, unlike its northern counterpart.

Main trunk

The distal portion of the ice stream (near transects G3 and G4) is undergoing the most dramatic changes. The northern margin is migrating inward, while the southern margin remains the same. A combination of narrowing, decelerating and increasing basal drag causes this area to thicken dramatically.

6.2. Potential cause

Evidence of both past (Clarke and Bentley, 1995; Jacobel and others, 1996; Nereson and Raymond, 2001) and current (Bindschadler and Vornberger, 1998; Echelmeyer and Harrison, 1998; Hamilton and others, 1998; Harrison and others, 1998; Jacobson and Raymond, 1998) margin migrations gives clues about the changing behavior of WIS. Ice-stream width is dictated by a balance between the entrainment of ridge ice and the advection of streaming ice. As Raymond and others (2001) posit, a decrease in basal velocity could cause a subsequent decrease in basal heat production inside the margin. This could cause streaming ice to be incorporated into the ridge, effectively narrowing the ice stream. This process explains the narrowing and deceleration at G3 and G4.

When the ice stream is widening and decelerating, as in G1n and G2n, the above shear-margin adjustment process does not apply. Here, the balance between entrainment and advection is perturbed by an external forcing, possibly a strengthening of the bed (Tulaczyk and others, 2000; Raymond and others, 2001; Joughin and others, 2002).

Several studies find that the majority of melt beneath the Siple Coast ice stream is produced near the onset of streaming (Raymond, 2000; Whillans and others, 2001) underneath the tributaries (Joughin and others, 1999, 2003; Price and others, 2002), with a possible contribution from subglacial lakes (Siegert and Bamber, 2000). Meanwhile, minimal melt (and potentially freeze-on) is found underneath the most active part of WIS, in modeled (Joughin and others, 2003; Vogel and others, 2003; this paper), theoretical (Raymond, 2000), and observed (Engelhardt and Kamb, 1993) accounts. Using a numerical model of basal melt patterns under the Siple Coast tributaries, Vogel and others (2003) infer a depletion of basal melt since the early Holocene. If this is the case, then depletion in basal meltwater should affect the terminus of the ice stream first. Less subglacial water could increase basal resistance (Clarke, 1987; Tulaczyk and others, 2000), and therefore could account for the observed deceleration (Stephenson and Bindschadler, 1988; Hulbe and Whillans, 1997; Bindschadler and Vornberger, 1998; Echelmeyer and Harrison, 1999; Joughin and others, 2002; Vogel and others, 2003; this paper).

We speculate that the depletion of meltwater at the base of the ice stream is most likely responsible for the observed changes. Ice streams may stop flowing fast if the lubricating conditions are lost (Tulaczyk and others, 2000), a hypothesized precursor to the shut-down of Kamb Ice Stream (Price and Whillans, 2001; Alley, 2002; Joughin and Tulaczyk, 2002). Not enough research has been done to say whether WIS is headed towards stagnation or not. However, there is mounting evidence of its current deceleration and a change in basal conditions.

ACKNOWLEDGEMENTS

This research was supported by a grant from NASA's Polar Oceans and Ice Sheets Program. This is Byrd Polar Research Center contribution No. C-1327. Photoblock velocity data were collected by the late I. Whillans as part of a project funded by the US Office of Polar Programs, National Science Foundation. Thanks to I. Joughin, A. Smith, R. Bindschadler and G. Hamilton for their helpful comments made during the review process.

REFERENCES

Alley, R.B. 2002. On thickening ice? *Science,* **295**(5554), 451–452.

Bindschadler, R. and W. Seider. 1998. Declassified intelligence satellite photography (DISP) coverage of Antarctica. *U.S. Nat. Aeron. Space Admin. Tech. Mem.* 1998-206879.

Bindschadler, R. and P. Vornberger. 1998. Changes in the West Antarctic ice sheet since 1963 from declassified satellite photography. *Science,* **279**(5351), 689–692.

Bindschadler, R.A., S.N. Stephenson, D.R. MacAyeal and S. Shabtaie. 1987. Ice dynamics at the mouth of Ice Stream B, Antarctica. *J. Geophys. Res.,* **92**(B9), 8885–8894.

Budd, W.F., D. Jenssen and U. Radok. 1971. Derived physical characteristics of the Antarctic ice sheet. *ANARE Interim Rep., Ser. A(IV), Glaciology* 120. (Meteorology Dept. Publ. 18.)

Clarke, G.K.C. 1987. Subglacial till: a physical framework for its properties and processes. *J. Geophys. Res.,* **92**(B9), 9023–9036.

Clarke, T.S. and C.R. Bentley. 1995. Evidence for a recently abandoned ice stream shear margin. *Eos,* **76**(46), Fall Meeting Supplement, F194.

Clarke, T.S. and C.R. Bentley. 2000. Evidence for a recently abandoned ice stream shear margin adjacent to Ice Stream B2, Antarctica, from ice-penetrating radar measurements. *J. Geophys. Res.,* **105**(B6), 13,409–13,422.

Echelmeyer, K.A. and W.D. Harrison. 1999. Ongoing margin migration of Ice Stream B, Antarctica. *J. Glaciol.,* **45**(150), 361–369.

Echelmeyer, K.A., W.D. Harrison, C. Larsen and J.E. Mitchell. 1994. The role of the margins in the dynamics of an active ice stream. *J. Glaciol.,* **40**(136), 527–538.

Engelhardt, H. and B. Kamb. 1993. Vertical temperature profile of Ice Stream B. *Antarct. J. U.S.,* **28**(5), Review 1993, 63–66.

Engelhardt, H., N. Humphrey, B. Kamb and M. Fahnestock. 1990. Physical conditions at the base of a fast moving Antarctic ice stream. *Science,* **248**(4951), 57–59.

Hamilton, G.S., I.M. Whillans and P.J. Morgan. 1998. First point measurements of ice-sheet thickness change in Antarctica. *Ann. Glaciol.,* **27**, 125–129.

Harrison, W.D., K.A. Echelmeyer and C.F. Larsen. 1998. Measurement of temperature in a margin of Ice Stream B, Antarctica: implications for margin migration and lateral drag. *J. Glaciol.,* **44**(148), 615–624.

Hulbe, C.L. and I.M. Whillans. 1997. Weak bands within Ice Stream B, West Antarctica. *J. Glaciol.,* **43**(145), 377–386.

Jackson, M. 1991. Repeat aerial photogrammetry of Ice Stream B, West Antarctica. (MSc thesis, Ohio State University, Columbus.)
Jackson, M. and B. Kamb. 1997. The marginal shear stress of Ice Stream B, West Antarctica. *J. Glaciol.,* **43**(145), 415–426.
Jacobel, R.W., T.A. Scambos, N.A. Nereson and C.F. Raymond. 2000. Changes in the margin of Ice Stream C, Antarctica. *J. Glaciol.,* **46**(152), 102–110.
Jacobson, H.P. and C.F. Raymond. 1998. Thermal effects on the location of ice stream margins. *J. Geophys. Res.,* **103**(B6), 12,111–12,122.
Jezek, K.C. 1999. Glaciological properties of the Antarctic ice sheet from RADARSAT-1 synthetic aperture radar imagery. *Ann. Glaciol.,* **29**, 286–290.
Jezek, K.C., H. Liu, Z. Zhao and B. Li. 1999. Improving a digital elevation model of Antarctica using radar remote sensing data and GIS techniques. *Polar Geogr.,* **23**(3), 185–200.
Joughin, I. 2002. Ice-sheet velocity mapping: a combined interferometric and speckle-tracking approach. *Ann. Glaciol.,* **34**, 195–201.
Joughin, I. and S. Tulaczyk. 2002. Positive mass balance of the Ross ice streams, West Antarctica. *Science,* **295**(5554), 476–480.
Joughin, I. *and 7 others*. 1999. Tributaries of West Antarctic ice streams revealed by RADARSAT interferometry. *Science,* **286**(5438), 283–286.
Joughin, I., S. Tulaczyk, R.A. Bindschadler and S. Price. 2002. Changes in West Antarctic ice stream velocities: observation and analysis. *J. Geophys. Res.,* **107**(B11), 2289. (10.1029/2001JB001029.)
Joughin, I.R., S. Tulaczyk and H.F. Engelhardt. 2003. Basal melt beneath Whillans Ice Stream and Ice Streams A and C, West Antarctica. *Ann. Glaciol.,* **36**, 257–262
Kamb, B. 1991. Rheological nonlinearity and flow instability in the deforming bed mechanism of ice stream motion. *J. Geophys. Res.,* **96**(B10), 16,585–16,595.
Kim, K. 1999. Application of time series satellite data to earth science problems. (MSc thesis, Ohio State University.)
Kim, K.T., K.C. Jezek and H.G. Sohn. 2001. Ice-shelf advance and retreat rates along the coast of Queen Maud Land, Antarctica. *J. Geophys. Res.,* **106**(C4), 7097–7106.
Liu, H., K.C. Jezek and B. Li. 1999. Development of an Antarctic digital elevation model by integrating cartographic and remotely sensed data: a geographic information system based approach. *J. Geophys. Res.,* **104**(B10), 23,199–23,213.
Lythe, M.B., D.G. Vaughan and BEDMAP consortium. 2000. *BEDMAP–bed topography of the Antarctic*. (Scale 1 : 10,000,000.) British Antarctic Survey. (BAS (Misc) 9, http://www.antarctica.ac.uk/aedc/bedmap/.)
McDonald, J. and I.M. Whillans. 1988. Comparison of results from Transit satellite tracking. *Ann. Glaciol.,* **11**, 83–88.
McDonald, J. and I.M. Whillans. 1992. Search for temporal changes in the velocity of Ice Stream B, West Antarctica. *J. Glaciol.,* **38**(128), 157–161.
Nereson, N.A. and C.F. Raymond. 2001. The elevation history of ice streams and the spatial accumulation pattern along the Siple Coast of West Antarctica inferred from ground-based radar data from three inter-ice-stream ridges. *J. Glaciol.,* **47**(157), 303–313.
Oppenheimer, M. 1998. Global warming and the stability of the West Antarctic ice sheet. *Nature,* **393**(6683), 325–332.
Price, S.F. and I.M. Whillans. 2001. Crevasse patterns at the onset to Ice Stream B, West Antarctica. *J. Glaciol.,* **47**(156), 29–36.
Price, S.F., R.A. Bindschadler, C.L. Hulbe and D.D. Blankenship. 2002. Force balance along an inland tributary and onset to Ice Stream D, West Antarctica. *J. Glaciol.,* **48**(160), 20–30.
Raymond, C.F. 2000. Energy balance of ice streams. *J. Glaciol.,* **46**(155), 665–674.
Raymond, C.F., K.A. Echelmeyer, I.M. Whillans and C.S.M. Doake. 2001. Ice stream shear margins. *In* Alley, R.B. and R.A. Bindschadler, *eds. The West Antarctic ice sheet: behavior and environment*. Washington, DC, American Geophysical Union, 137–155. (Antarctic Research Series 77.)
Retzlaff, R., N. Lord and C.R. Bentley. 1993. Airborne-radar studies: Ice Streams A, B and C, West Antarctica. *J. Glaciol.,* **39**(133), 495–506.
Rose, K.E. 1979. Characteristics of ice flow in Marie Byrd Land, Antarctica. *J. Glaciol.,* **24**(90), 63–75.
Shabtaie, S. and C.R. Bentley. 1988. Ice-thickness map of the West Antarctic ice streams by radar sounding. *Ann. Glaciol.,* **11**, 126–136.
Shabtaie, S., I.M. Whillans and C.R. Bentley. 1987. The morphology of Ice Streams A, B, and C, West Antarctica, and their environs. *J. Geophys. Res.,* **92**(B9), 8865–8883.
Shabtaie, S., C.R. Bentley, R.A. Bindschadler and D.R. MacAyeal. 1988. Mass-balance studies of Ice Streams A, B, and C, West Antarctica, and possible surging behavior of Ice Stream B. *Ann. Glaciol.,* **11**, 137–149.
Siegert, M.J. and J.L. Bamber. 2000. Subglacial water at the heads of Antarctic ice-stream tributaries. *J. Glaciol.,* **46**(155), 702–703.
Spikes, V.B., B.M. Csathó, G.S. Hamilton and I.M. Whillans. 2003. Thickness changes on Whillans Ice Stream and Ice Stream C, West Antarctica, derived from laser altimeter measurements. *J. Glaciol.,* **49**(165), 223–230.
Stephenson, S.N. and R.A. Bindschadler. 1988. Observed velocity fluctuations on a major Antarctic ice stream. *Nature,* **334**(6184), 695–697.
Thomas, R.H. and C.R. Bentley. 1978. The equilibrium state of the eastern half of the Ross Ice Shelf. *J. Glaciol.,* **20**(84), 509–518.
Tulaczyk, S.M., B. Kamb and H.F. Engelhardt. 2000. Basal mechanics of Ice Stream B, West Antarctica. II. Undrained-plastic-bed model. *J. Geophys. Res.,* **105**(B1), 483–494.
Van der Veen, C.J. 1999. *Fundamentals of glacier dynamics*. Rotterdam, etc., A.A. Balkema Publishers.
Van der Veen, C.J. and I.M. Whillans. 1989. Force budget: I. Theory and numerical methods. *J. Glaciol.,* **35**(119), 53–60.
Van der Veen, C.J. and I.M. Whillans. 1996. Model experiments on the evolution and stability of ice streams. *Ann. Glaciol.,* **23**, 129–137.
Venteris, E.R. and I.M. Whillans. 1998. Variability of accumulation rate in the catchments of Ice Streams B, C, D and E, Antarctica. *Ann. Glaciol.,* **27**, 227–230.
Vogel, S.W., S. Tulaczyk and I.R. Joughin. 2003. Distribution of basal melting and freezing beneath tributaries of Ice Stream C: implication for the Holocene decay of the West Antarctic ice sheet. *Ann. Glaciol.,* **36**, 273–282
Vornberger, P.L. and I.M. Whillans. 1990. Crevasse deformation and examples from Ice Stream B, Antarctica. *J. Glaciol,* **36**(122), 3–10.
Whillans, I.M. and R.A. Bindschadler. 1988. Mass balance of Ice Stream B, West Antarctica. *Ann. Glaciol.,* **11**, 187–193.
Whillans, I.M. and C.J. van der Veen. 1993. New and improved determinations of velocity of Ice Streams B and C, West Antarctica. *J. Glaciol.,* **39**(133), 483–490.
Whillans, I.M. and C.J. van der Veen. 1997. The role of lateral drag in the dynamics of Ice Stream B, Antarctica. *J. Glaciol.,* **43**(144), 231–237.
Whillans, I.M., M. Jackson and Y.-H. Tseng. 1993. Velocity pattern in a transect across Ice Stream B, Antarctica. *J. Glaciol.,* **39**(133), 562–572.
Whillans, I.M., C.R. Bentley and C.J. van der Veen. 2001. Ice Streams B and C. *In* Alley, R.B. and R.A. Bindschadler, *eds. The West Antarctic ice sheet: behavior and environment*. Washington, DC, American Geophysical Union, 257–281. (Antarctic Research Series 77.)

APPENDIX

The mass balance was calculated along each transect shown in Figure 3. The results are listed in Tables A1 and A2. In some cases where the area between the flux

Table A1. Photoblock mass-balance variables. F_i is the flux in through the upstream gate, S is the surface area in between the two flux gates, b is the area-averaged accumulation rate, F_s is the flux through the ice surface (accumulation rate times the surface area), F_{in} is the sum of F_i and F_s, F_{out} is the flux out of the downstream gate, and dH/dt is the rate of thickness change. The north tributary refers to the Whillans Ice Stream; the south tributary refers to Van der Veen Ice Stream; 'all' refers to the sum of both Ice Streams

Flow area	Tributary	F_i $10^{12}\,kg\,a^{-1}$	S $10^{6}\,m^{2}$	b $m\,a^{-1}$	F_s $10^{10}\,kg\,a^{-1}$	F_{in} $10^{12}\,kg\,a^{-1}$	F_{out} $10^{12}\,kg\,a^{-1}$	dH/dt $mm\,a^{-1}$
G1–G2	WIS1 north	10.39 ± 0.43	591 ± 25	0.12 ± 0.01	6.50 ± 0.61	10.45 ± 0.43	10.73 ± 0.45	–516.7 ± 271.5
G1–G2	WIS2 south	12.13 ± 0.68	855 ± 25	0.12 ± 0.01	9.41 ± 0.83	12.22 ± 0.68	12.12 ± 0.56	127.5 ± 384.3
G1–G2	WIS all	22.52 ± 0.80	1446 ± 25	0.12 ± 0.01	15.91 ± 1.35	22.67 ± 0.80	22.85 ± 0.51	–135.7 ± 414.4
G2–G3	WIS1 north	10.73 ± 0.45	1827 ± 25	0.11 ± 0.01	18.43 ± 1.69	10.90 ± 0.45	11.62 ± 0.51	–429.8 ± 296.8
G2–G3	WIS2 south	12.12 ± 0.56	1885 ± 25	0.11 ± 0.01	19.0 ± 1.75	12.39 ± 0.56	13.09 ± 0.54	–405.0 ± 339.4
G2–G3	WIS all	22.85 ± 0.72	3712 ± 25	0.11 ± 0.01	37.44 ± 3.41	23.20 ± 0.72	24.72 ± 0.53	–446.5 ± 388.4
G3–G4	WIS1 north	11.62 ± 0.51	1268 ± 25	0.10 ± 0.01	12.79 ± 1.30	11.75 ± 0.51	12.57 ± 0.56	–705.2 ± 330.4
G3–G4	WIS2 south	13.09 ± 0.54	1105 ± 25	0.10 ± 0.01	11.15 ± 1.14	13.20 ± 0.54	13.04 ± 0.61	157.9 ± 355.4
G3–G4	WIS all	24.71 ± 0.74	2417 ± 25	0.10 ± 0.01	22.16 ± 2.23	24.94 ± 0.74	25.61 ± 0.59	–302.3 ± 412.5

Table A2. InSAR mass-balance variables

Flow area	Tributary	F_i $10^{12}\,kg\,a^{-1}$	S $10^{6}\,m^{2}$	b $m\,a^{-1}$	F_s $10^{10}\,kg\,a^{-1}$	F_{in} $10^{12}\,kg\,a^{-1}$	F_{out} $10^{12}\,kg\,a^{-1}$	dH/dt $mm\,a^{-1}$
G0–G1	WIS1 north	9.39 ± 0.68	2463 ± 25	0.13 ± 0.01	29.36 ± 2.28	9.68 ± 0.68	10.20 ± 0.43	–230.2 ± 351.1
G0–G1	WIS2 south	12.18 ± 0.78	2233 ± 25	0.13 ± 0.01	26.62 ± 2.07	12.49 ± 0.78	11.73 ± 0.68	371.2 ± 449.8
G0–G1	WIS all	21.57 ± 1.03	4696 ± 25	0.13 ± 0.01	55.98 ± 4.32	22.13 ± 1.03	21.93 ± 0.56	46.4 ± 511.1
G1–G2	WIS1 north	10.20 ± 0.54	591 ± 25	0.12 ± 0.01	6.50 ± 0.61	10.26 ± 0.54	10.46 ± 0.56	–369.0 ± 339.4
G1–G2	WIS2 south	11.73 ± 1.15	855 ± 25	0.12 ± 0.01	9.41 ± 0.83	11.80 ± 1.15	11.93 ± 0.62	–165.8 ± 569.9
G1-G2	WIS all	21.93 ± 1.27	1446 ± 25	0.12 ± 0.01	15.91 ± 1.35	22.06 ± 1.27	22.39 ± 0.59	–248.9 ± 611.1
G2–G3	WIS1 north	10.46 ± 0.56	1827 ± 25	0.11 ± 0.01	18.43 ± 1.69	10.64 ± 0.56	10.68 ± 0.68	–23.9 ± 383.3
G2–G3	WIS2 south	11.93 ± 0.62	1885 ± 25	0.11 ± 0.01	19.00 ± 1.75	12.12 ± 0.62	12.90 ± 0.53	–451.2 ± 355.9
G2–G3	WIS all	22.39 ± 0.84	3712 ± 25	0.11 ± 0.01	37.44 ± 3.41	22.76 ± 0.84	23.62 ± 0.60	–252.7 ± 449.8
G3–G4	WIS1 north	10.68 ± 0.68	1268 ± 25	0.10 ± 0.01	12.79 ± 1.30	10.81 ± 0.68	10.52 ± 0.51	249.4 ± 369.8
G3–G4	WIS2 south	12.90 ± 0.53	1105 ± 25	0.10 ± 0.01	11.15 ± 1.14	13.01 ± 0.53	12.06 ± 0.62	937.5 ± 355.8
G3–G4	WIS all	23.62 ± 0.86	2417 ± 25	0.10 ± 0.01	22.16 ± 2.23	23.84 ± 0.86	22.58 ± 0.57	568.5 ± 448.9

gates is small, the error is larger than the result. Tables A1 and A2 list all of the results, but in analyzing them, some gates are combined in order to obtain statistically meaningful results.

In all calculations, the flux in and out of the gates is a product of the ice velocity, the ice thickness as determined by Shabtaie and Bentley (1988) and the density of ice ($917\,kg\,m^{-3}$).

MS received 11 January 2004 and accepted in revised form 14 October 2004